Quaternary Science Reviews 249 (2020) 106563

Contents lists available at ScienceDirect

Quaternary Science Reviews

journal homepage: www.elsevier.com/locate/quascirev

Paleoceanographic changes in the Southern Ocean off Elephant Island since the last glacial period: Links between surface water productivity, nutrient utilization, bottom water currents, and ice-rafted debris

Sunghan Kim [a], Kyu-Cheul Yoo [a,*], Jae Il Lee [a], Youn Ho Roh [a,b], Young-Suk Bak [c], In-Kwon Um [d], Min Kyung Lee [a], Ho Il Yoon [a]

[a] Korea Polar Research Institute, Incheon, 21990, South Korea
[b] University of Science and Technology, Daejeon, 34113, South Korea
[c] Department of Earth and Environmental Sciences, Jeonbuk National University, Jeonju, 54896, South Korea
[d] Petroleum and Marine Research Division, Korea Institute of Geoscience and Mineral Resources, Daejeon, 34132, South Korea

A R T I C L E I N F O

Article history:
Received 6 April 2020
Received in revised form
20 August 2020
Accepted 22 August 2020
Available online 25 September 2020

Keywords:
Paleoceanography
Marine core
Geochemistry
Nutrient utilization
Ocean-cryosphere interaction
Ice-rafted debris

A B S T R A C T

To understand past changes in ocean–cryosphere interactions in the Southern Ocean off the Antarctic Peninsula, multi-proxy analyses of three sediment cores located off Elephant Island were used to reconstruct changes in paleoproductivity, nutrient utilization, bottom current intensity, and iceberg calving since the last glacial period. The glacial period was characterized by low surface water productivity with high nutrient utilization, indicating surface water stratification. During the deglaciation, surface water productivity increased with decreasing nutrient utilization, implying that the increase is associated with increased nutrient supply from the subsurface water by enhancing Antarctic Circumpolar Current (ACC) influence as fronts migrate southward with warming. Abundant occurrence of grains >1 mm during the deglacial period indicates rapid ice sheet retreat with large-scale melting and calving. During the glacial period, however, coarse silt–fine sand-sized fraction represented ice-rafted debris (IRD). The different IRD grain size characteristics are thought to be related to the IRD source material characteristics. Regardless of IRD input, the running downcore correlation (5 to 9-point) between sortable silt mean grain size and percentage showed that sediments are well sorted by bottom current. However, the cross plot of them showed different temporal relationships. Sediments were sorted by the ACC and southwestward flowing bottom current. Along with southward migration of fronts and the ACC, southwestward flowing bottom current influence diminished, whereas the ACC influence increased particularly from 7 ka. Our results indicate that the sedimentary processes in the Scotia Sea largely depend on the regional interactions between the ocean and the cryosphere.

1. Introduction

The Southern Ocean is divided into the Antarctic Zone (AZ), Polar Front Zone (PFZ), and Subantarctic Zone (SAZ) (Tréguer and Jacques, 1992; Orsi et al., 1995). Sediment traps and surface sediments along a latitudinal transect showed a close link between Southern Ocean zonation and the total mass flux and composition of sediments (e.g., Honjo et al., 2000; Cárdenas et al., 2019). The position of each zone varies with the latitudinal displacement of the Southern Ocean fronts, which migrate equatorward during cold periods and poleward during warm periods (Gersonde et al., 2005; Kemp et al., 2010; Manoj and Thamban, 2015; Roberts et al., 2017). These frontal migrations can alter the surface oceanography and influence surface water productivity. The latitudinal difference between the Polar Front (PF) and the Southern Boundary of the Antarctic Circumpolar Current (SBACC) narrows toward the Drake Passage. In addition, the SBACC is related to the extent of the winter sea-ice field (Orsi et al., 1995). Therefore, the northernmost Antarctic Peninsula (AP) is an ideal location to assess changes in surface water conditions in response to frontal/sea-ice variability since the last glacial period.

The estimates of biogenic opal productivity from the Scotia Sea

* Corresponding author.
E-mail address: kcyoo@kopri.re.kr (K.-C. Yoo).

https://doi.org/10.1016/j.quascirev.2020.106563
0277-3791/

since the last glacial period implied a dominance of open-ocean species (e.g., *Fragilariopsis kerguelensis*) during high opal productivity and a dominance of *Eucampia Antarctica* (a dominant glacial species) during low productivity (Burckle and Burak, 1988; Bak et al., 2010, 2014; Xiao et al., 2016). Export production was found to be relatively low during the last glacial maximum (LGM) in the southern Scotia Sea (e.g., Yoon et al., 2007). Sedimentary records from the south Orkney Plateau covering the last 8600 years showed a weakened correlation between biogenic opal and total organic carbon (TOC) after 5 ka (Lee et al., 2010). However, the coupling of biogenic opal and export production in the Scotia Sea since the last glacial period remains inconclusive due to the absence of TOC records. Despite the high biogenic opal production in the Scotia Sea (e.g., Bak et al., 2010; Sprenk et al., 2013; Xiao et al., 2016), the relationship between nutrient utilization and primary production since the last glacial period is unknown. As a result, surface-subsurface water mass exchanges and the controlling mechanisms on surface water productivity since the last glacial remains unclear.

Diatom records from Scotia Sea sediment cores imply an expansion of sea ice during glacial periods (Gersonde et al., 2005; Bak et al., 2010, 2014; Collins et al., 2012; Xiao et al., 2016). Bentley et al. (2014) showed that the grounding line advanced to the continental shelf break in the northern AP at ca. 20 ka, which subsequently retreated in conjunction with increasing global sea level. The sequential sedimentological changes in response to the glacial retreat are likely to be recorded in Scotia Sea sediments. Previously, only the presence of coarse grains (>1 or 2 mm) (e.g., Diekmann et al., 2000; Weber et al., 2012) were interpreted as ice-rafted debris (IRD) in sediment records of the Scotia Sea; however, a recent study shed new light on the grain size distribution of IRD in sediments that coarse silt—fine sand fractions are dominant (Kim et al., 2018a). Analysis of the sedimentary IRD footprint can highlight the depositional processes of IRD in response to oceanographic changes. Moreover, past cryospheric changes in Antarctica likely influenced bottom water conditions due to the presence of numerous deep/bottom water currents in the Scotia Sea (Orsi et al., 1995; Hernández-Molina et al., 2006).

In this study, we present downcore records of surface water productivity (biogenic opal and TOC concentrations), nutrient utilization ($\delta^{15}N$), sedimentology (grain size and abundance of >1 mm), physical property (magnetic susceptibility (MS), and water content (WC)) from three sediment cores off Elephant Island in the Southern Ocean. They are also supported by the diatom assemblage. We aim to reconstruct and assess the relationships between 1) surface water productivity, 2) nutrient utilization, 3) bottom current intensity, and 4) iceberg calving since the last glacial period.

2. Study area

The eastward flowing Antarctic Circumpolar Current (ACC) dominates oceanic circulation in the Scotia Sea, which is located in the Atlantic sector of the Southern Ocean (Fig. 1). The ACC is the world's largest current (Donohue et al., 2016) and consists of various water masses with a total transport volume of >173.3 Sverdrup (1 Sv = 10^6 m^3S^{-1}).

The occurrence of phytoplankton blooms and begins starts in early spring as the surface water column stabilizes in response to melting ice (Fryxell and Kendrick, 1988). The spatial distribution of phytoplankton is strongly influenced by frontal systems, the sea ice edge, and grazing pressure (Tréguer et al., 1991; Socal et al., 1997). The Antarctic PF and the northern limit of seasonal sea ice are characterized by high biosiliceous production rates (Geibert et al., 2005; Diekmann, 2007), and the SBACC is related to the limit of the winter sea ice field (Xiao et al., 2016).

The Scotia Sea receives terrestrial sediments by ice rafting, oceanic currents, and eolian input (Diekmann et al., 2000; Ó Cofaigh et al., 2001; Weber et al., 2014; Kim et al., 2018a). The Scotia Sea is located at the extension of Iceberg Alley (Anderson and Andrew, 1999)—a zone of highest iceberg transport from the Weddell Sea. In addition, the Scotia Sea is the most likely location for detecting icebergs based on ALTIBERG database observations (Tournadre et al., 2015) and modeling results (Merino et al., 2016). The Scotia Sea is influenced by the Weddell Sea Deep Water (WSDW) and ACC, consequently the bottom water transport of sediment is important. Various contourite drifts in the Scotia Sea and northwestern Weddell Sea have been reported from Holocene sediments (e.g., Gilbert et al., 1998; Maldonado et al., 2003; Yoon et al., 2007).

3. Material and methods

Sediment cores GC03-C1, BC03-C1 (60°27′S, 55°42′W, 3774 m depth, 892 cm length for GC03-C1 and 32 cm length for BC03-C1), GC03-C2 (60°34′S, 55°55′W, 3750 m depth, 834 cm length), and GC03-C4 (60°33′S, 55°52′W, 3778 m depth, 840 cm length) were collected from the southern Scotia Sea off Elephant Island onboard the *R/V Yuzhmorgeologiya* during the 2003/2004 Korea Antarctic Research Program (Fig. 1). All cores were opened, described, and sub-sampled at the Korea Polar Research Institute (KOPRI), South Korea.

3.1. Physical properties (MS and WC)

The MS values for all cores were measured at 1 cm intervals on split half core sections using a Bartington MS-2B susceptibility meter at KOPRI. The MS values for GC03-C1 and GC03-C2 were reported in Bak et al. (2010) and Bak et al. (2014), respectively. The MS values for GC03-C4 were reported in Kim et al. (2018a). WC for all cores was measured at 4 cm intervals on 1 cm thick sub-samples. WC was calculated using the following equation.

$$\mathrm{WC}\ (\%) = (\text{mass of wet sediment} - (\text{mass of dry sediment} + \text{mass of salt}))\ /\ \text{mass of wet sediment} \times 100$$

3.2. Geochemical proxies (biogenic opal, TOC, and $CaCO_3$ concentrations)

The geochemical proxies for all cores were measured at 2 cm intervals on 1 cm thick sub-samples; however, biogenic opal for cores GC03-C2 and GC03-C4 was measured at 4 cm intervals. Biogenic silica concentrations were measured using a Continuous Flow Analyzer (SKALAR SANplus Analyzer) by the wet-alkaline extraction method modified from DeMaster (1981) at KOPRI (Kim et al., 2018b). Biogenic opal concentrations were calculated by multiplying biogenic silica concentrations by 2.4 (Mortlock and Froelich, 1989), and the relative error of biogenic silica

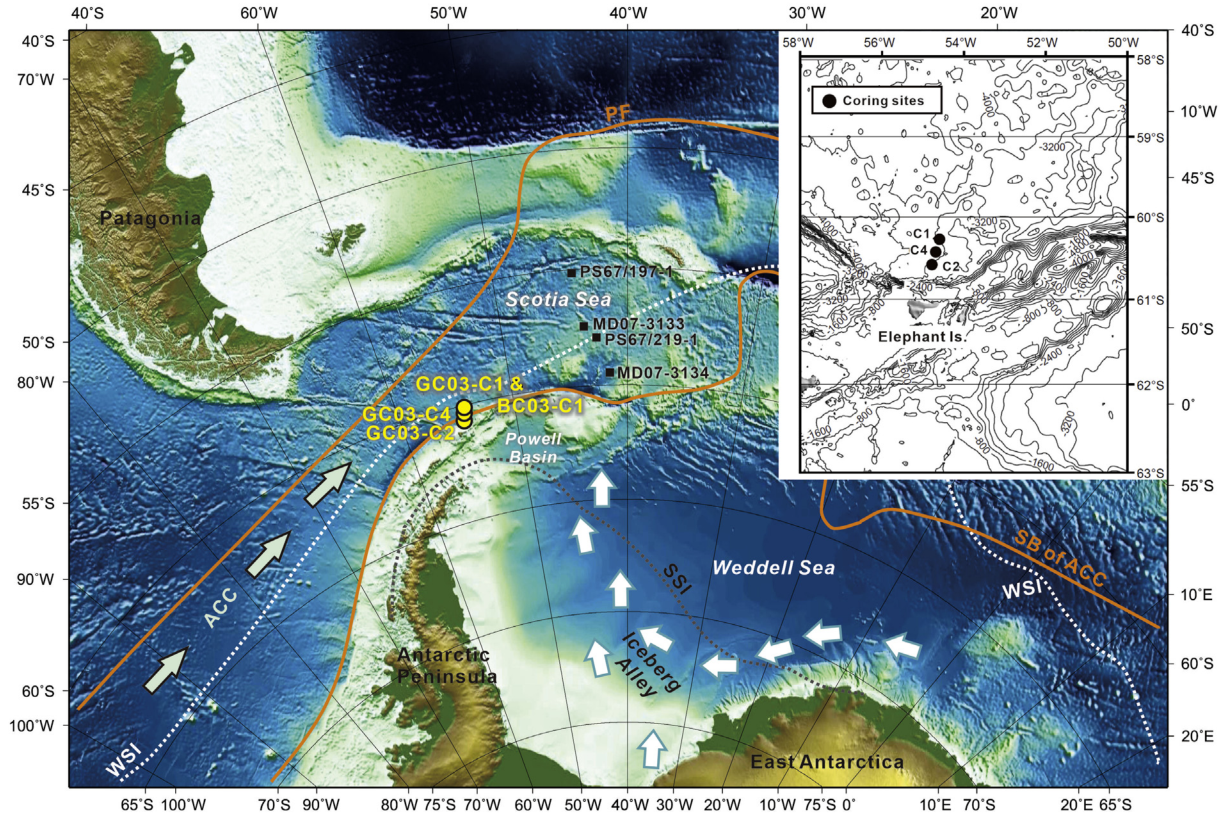

Fig. 1. (a) Map of the study region indicating the locations of the sediment cores examined in this study as well as in previous investigations. The white open arrows indicate the location of iceberg alley (from Anderson and Andrew, 1999); the orange lines indicate the Polar Front (PF) and the Southern Boundary of the Antarctic Circumpolar Current (SBACC; Orsi et al., 1995); the dark gray and white dashed lines indicate the summer (SSI) and winter (WSI) sea ice extent, respectively (Gersonde et al., 2005); and the light green arrows indicate the ACC.

concentrations was <1%. Total inorganic carbon (TIC) concentrations were measured using a UIC CO_2 coulometer (Model CM5240) at KOPRI, and the relative standard deviation was ±0.1%. $CaCO_3$ concentrations were calculated by multiplying TIC concentrations by 8.333, and the relative standard deviation was ±1%. Total carbon (TC) concentrations were measured by an Organic Elemental Analyzer (FLASH 2000 NC Analyzer) with an analytical precision of less than ±0.1%. TOC concentration was calculated as the difference between TC and TIC.

3.3. $\delta^{15}N$ values

$\delta^{15}N$ ($\delta^{15}N_{acid}$) values for GC03-C1 were measured at 4 cm intervals following sediment treatment with 20% HCl. To compare $\delta^{15}N_{acid}$ and bulk $\delta^{15}N$, we measured bulk $\delta^{15}N$ values from 27 horizons covering a range (low to high) of $\delta^{15}N_{acid}$ values.

Bulk $\delta^{15}N$ values for GC03-C2 were measured at 4 cm intervals. All $\delta^{15}N$ values were measured using an EA–IRMS (Europa Scientific RoboPrep-CN elemental analyzer & Europa Scientific 20-20 mass spectrometer) at Iso-Analytical Ltd., UK. Nitrogen isotope ratios are expressed in the conventional delta notation, which is the per mil deviation from atmospheric nitrogen. The precision for nitrogen isotopes was approximately ±0.2‰.

3.4. Grain size analysis and count of grains>1 mm

We removed all biogenic components—including biogenic opal, organic matter, and $CaCO_3$—from the bulk sediments using sodium hydroxide, hydrogen peroxide, and hydrochloric acid, respectively. The grain size was then analyzed at 8 cm intervals for all cores using a laser diffraction particle analyzer (Microtrac S3500) at the Korea Institute of Geoscience and Mineral Resources. We classified the sediments following the scheme by Folk and Ward (1957). The mean grain size (MGS) within the range of 10–63 μm was calculated for sortable silt (SS: 10–63 μm). The volume percentages for 10 and 63 μm were calculated by interpolation of the two nearest values, as suggested in McCave and Andrews (2019).

We took X-radiographs of center slices (1 cm thick x 5 cm width x 30 cm length) removed from each core section. Finally, grains >1 mm in diameter were manually counted every 1 cm on the X-radiographs.

3.5. Diatom assemblage

Diatom assemblages for GC03-C1 are reported in Bak et al. (2010); assemblages were analyzed at 4 cm intervals in the above 316 cm interval which has low MS values and were analyzed at 12 cm intervals in the below 316 cm interval which has high MS values. Up to 200 diatom valves were counted per sample; *Chaetoceros* resting spores were excluded in the specimen count. Diatom assemblages in GC03-C2 are reported in Bak et al. (2014). To understand the general changes in the surface water environment since the LGM, the dominant diatom species that appeared in GC03-C1 were counted in GC03-C2 (Bak et al., 2014). As *Chaetoceros* resting spores in GC03-C2 were not counted and not presented in Bak et al. (2014), we counted the *Chaetoceros* resting spores for GC03-C2 in this study using the same diatom slides. The total diatom abundance of GC03-C1 and GC03-C2 is *Chaetoceros*-free.

4. Age model

The age model for cores GC03-C1 was established by combination of AMS ^{14}C dates of acid insoluble organic matter (AIOM) and MS correlation with the European Project for Ice Coring in Antarctica (EPICA) Dronning Maud Land (EDML) ice core nssCa^{2+} record (Shin et al., 2020). AIOM AMS ^{14}C dates were corrected by the box core top age and calibrated with no local reservoir age ($\Delta R = 0$) using CALIB 7.1 software (Stuiver and Reimer, 1993Stuiver and Reimer, 1993) with the MARINE13 dataset (Reimer et al., 2013Reimer et al., 2013) following Lee et al. (2010). Six AIOM AMS ^{14}C dates were used as tie points from the interval of <15 ka. From the high MS interval of >12.5 ka, seven tie points were set by the MS-EDML dust record correlations together with comparisons to the MS values of MD07-3133 and MD07-3134 in the Scotia Sea (Weber et al., 2012). The two cores are highly correlated to the EDML dust record and have very high sedimentation rates.

The age model for GC03-C2 was also established by combination of AMS ^{14}C dates of AIOM and MS correlation with the EDML ice core nssCa^{2+} record (Kim et al., 2018a). The age model for GC03-C4 was established by MS correlation with GC03-C2 (Kim et al., 2018a).

5. Results

5.1. Geochemical and physical proxies and bulk $\delta^{15}N$

We observed high MS values for all cores prior to 17.6 ka at >200 10^{-6} x CGS; this decreased to $<100 \times 10^{-6}$ CGS after 15 ka (Fig. 2). Trends in biogenic opal, TOC concentrations, and WC co-varied and showed opposite trends to the MS variability, with lower values before 17.6 ka and increasing values across the transition period corresponding to the deglacial period (17.6–10 ka) (Fig. 2). We identified no significant differences in TOC concentrations between the three cores; however, biogenic opal concentrations of GC03-C1 were generally 10% higher than those of cores GC03-C2 and GC03-C4 (Fig. 2). Biogenic opal concentrations in cores GC03-C2 and GC03-C4 gradually decreased from 7 ka (Fig. 2). TOC concentrations reached a maximum at 15 ka; this was followed by a decrease until 7 ka, after which the values remained constant (<0.5%) (Fig. 2). The C/N ratios of the three cores showed similar variability to MS, with high values (>10) before 17.6 ka and a decreasing trend (to <10) thereafter 17.6 ka, though some values were out-ranged (Fig. 2). The C/N ratios from GC03-C1 after 15 ka is generally lower than those of cores GC03-C2 and GC03-C4 (Fig. 2). We observed higher (>6‰) bulk $\delta^{15}N$ values before 17.6 ka in GC03-C2, which was followed by a gradual decrease to 3‰ (Fig. 2). $\delta^{15}N_{acid}$ values for GC03-C1 are ~1‰ lower than those of GC03-C2; however, both cores showed a similar variation pattern, with higher values (4–5‰) before 17.6 ka and a gradual decrease to 2‰ thereafter (Fig. 2). We observed a significant correlation between bulk $\delta^{15}N$ and $\delta^{15}N_{acid}$ for GC03-C1 ($r^2 = 0.94$, $n = 27$). The results are provided in Supplementary information 1.

5.2. Grain size and abundance of grain >1 mm

Grain size analysis showed coarser MGS (>30 μm) before 17.6 ka in all three cores; this was followed by a decrease to 15 μm until 15 ka. MGS then gradually coarsened toward the core top (up to 20 μm) and was accompanied by an increasing proportion of silt (Fig. 3). The sand fraction for all three cores co-varied and was

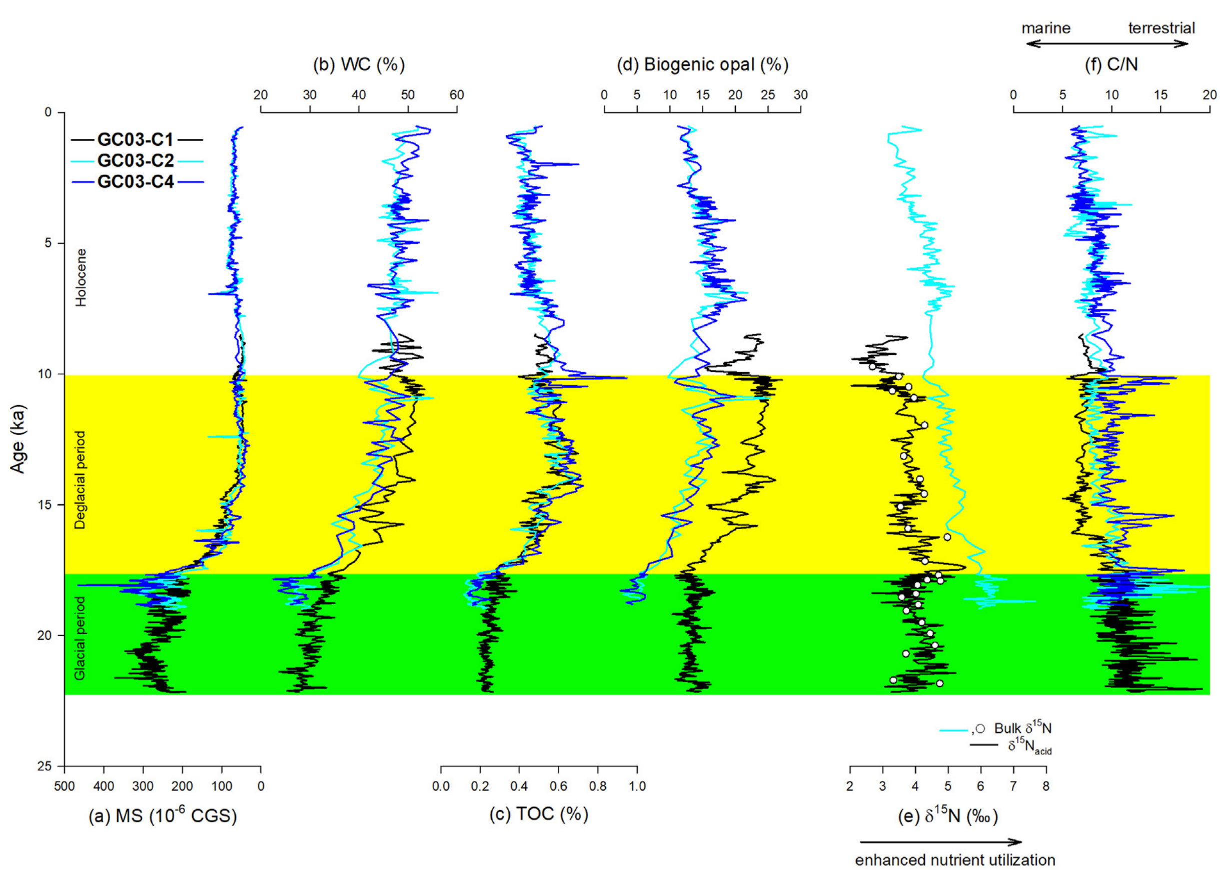

Fig. 2. Downcore profiles of (a) MS, (b) WC, (c) TOC concentration, (d) $\delta^{15}N$, and (e) C/N ratios of cores GC03-C1 (black), -C2 (cyan), and -C4 (blue).

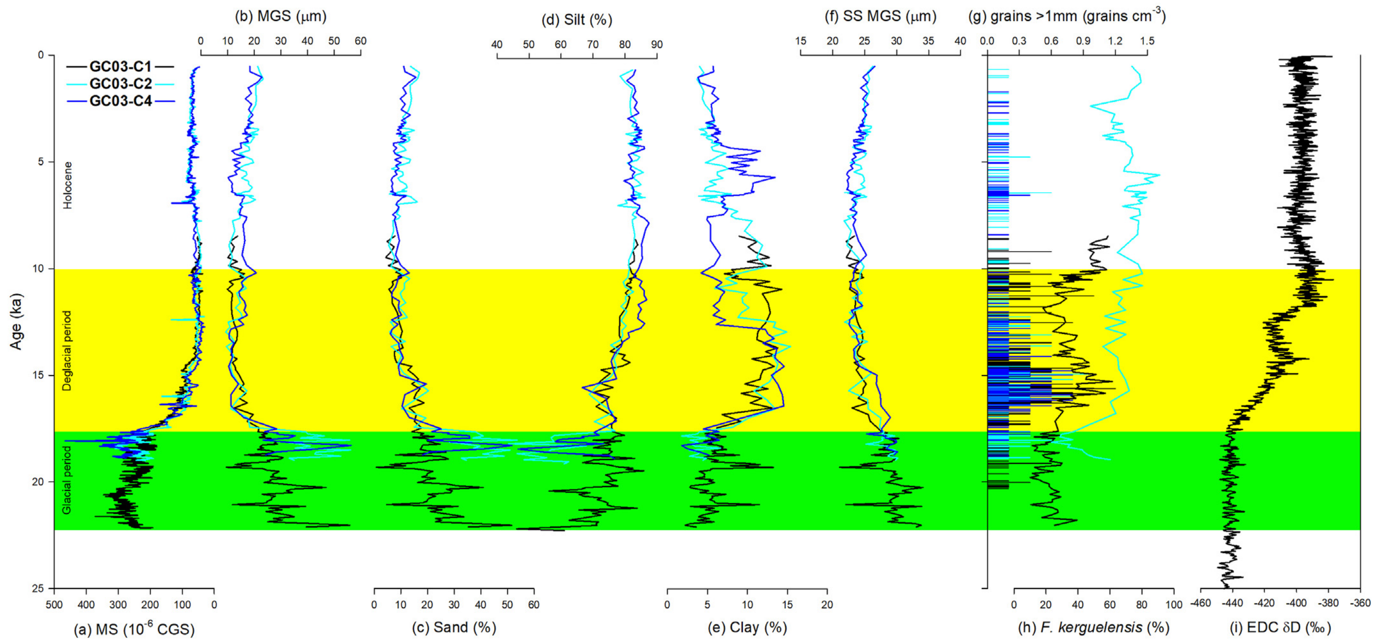

Fig. 3. Downcore profiles of (a) MS, (b) mean grain size (MGS), (c) sand proportion, (d) silt proportion, (e) clay proportion, (f) sortable silt MGS, and (g) abundance of grains >1 mm per cm^3 of cores GC03-C1 (black), -C2 (cyan), and -C4 (blue); (h) the relative abundance of open ocean diatom *F. kerguelensis* in GC03-C1 (Bak et al., 2010) and GC03-C2 (Bak et al., 2014); and (i) the EDC δD ice core record (Jouzel et al., 2007).

comparable to the MS trend, with higher values (>20%) before 17.6 ka followed by a subsequent decrease to <10% until 15 ka (Fig. 3). The silt fraction for all cores was lower before 17.6 ka, which then increased with decreasing MS and sand fraction until 15 ka; this continued to increase to almost 80% (Fig. 3). The clay fraction was low (<6%) before 17.6 ka, and sharply increased to 15% at 17.6 ka; this was followed by a gradual decrease to <6% (Fig. 3). SS MGS decreased from >30 μm during the glacial period to 23 μm at 7 ka; it then increased up-core to 27 μm. Grains >1 mm occurred throughout the records in all three cores, but were most abundant from 17.6 ka to 9 ka (Fig. 3). The results are provided in Supplementary information 1.

5.3. Diatom assemblage

Diatom assemblage of GC03-C1 was reported in Bak et al. (2010). Total diatom valves were low (<4 × 10^7/g) in the high MS interval before 17.6 ka, whereas were high (>10 × 10^7/g) in the low MS interval after 15 ka (Fig. 4). High MS intervals are characterized by low relative abundance of *F. kerguelensis* (20%) and high relative abundances of *Actinocyclus actinochilus* (15%) and *E. antarctica* var. *recta* (20%), whereas low MS intervals are characterized by high relative abundance of *F. kerguelensis* (80%) and low relative abundances of *A. actinochilus* (<5%) and *E. antarctica* var. *recta* (<5%). *Chaetoceros* resting spores showed high abundances (up to 80 × 10^6 valves/g) during 15 to 10 ka (Fig. 4).

Diatom assemblage of GC03-C2 was reported in Bak et al. (2014). Like GC03-C1, total diatom valves were low (<2 × 10^7/g) in the high MS interval before 17.6 ka, whereas were high (>6 × 10^7/g) in the low MS interval after 17.6 ka (Fig. 4). The high MS interval is characterized by low relative abundance of *F. kerguelensis* and high relative abundance of *A. actinochilus*, whereas the low MS interval is characterized by the opposite (Fig. 4). Trace amounts of *Chaetoceros* resting spores were observed in GC03-C2 before 17.6 ka; they reached a maximum abundance (25 × 10^6 valves/g) at 11 ka and began to decrease from 7 ka (Fig. 4). We observed similar variations in *Chaetoceros* resting spore abundance for both GC03-C2 and GC03-C1, but *Chaetoceros* resting spores are much higher in GC03-C1. The diatom data shown in this study are provided in Supplementary information 1.

6. Discussion

6.1. Variability in surface water productivity and nutrient utilization

As biogenic opal concentrations showed similar variability to total diatom abundance ($r^2 = 0.67$, $n = 127$, $p < 0.05$ for GC03-C1 and $r^2 = 0.47$, $n = 41$, $p < 0.05$ for GC03-C2) (Fig. 5), we assume that changes in biogenic opal concentrations reflect changes in diatom productivity change, which is consistent with previous studies (Xiao et al., 2016). Relatively lower r^2 value with a lower regression slope for GC03-C2 than GC03-C1 can be thought to be due to underestimation of total diatom counts (Fig. 5). The total diatom counts could be underestimated by not including *Chaetoceros* resting spores in this study. Because the correlation does not become significantly better by including *Chaetoceros* resting spores to total diatom counts, it is considered not the main reason. In addition, the abundance of total diatom values and *Chaetoceros* resting spores in both cores are consistent with previously reported values from the same region (Crosta et al., 1997). Because diatom preservation status is often related to diatom abundance and/or biogenic opal concentration, the lower total diatom counts and *Chaetoceros* resting spores of GC03-C2 are considered to be related to lower biogenic opal concentrations. Considering different methods for both biogenic opal concentration and diatom assemblage analysis, r^2 of 0.47 is considered as a good correlation.

There was a good correlation between biogenic opal and TOC concentrations in all three cores ($r = 0.90$, $n = 447$ for GC03-C1, $r = 0.74$, $n = 201$ for GC03-C2, and $r = 0.65$, $n = 210$ for GC03-C4 with $p < 0.05$ for all cores), indicating that diatom production had dominated the total primary production in the southern Scotia Sea

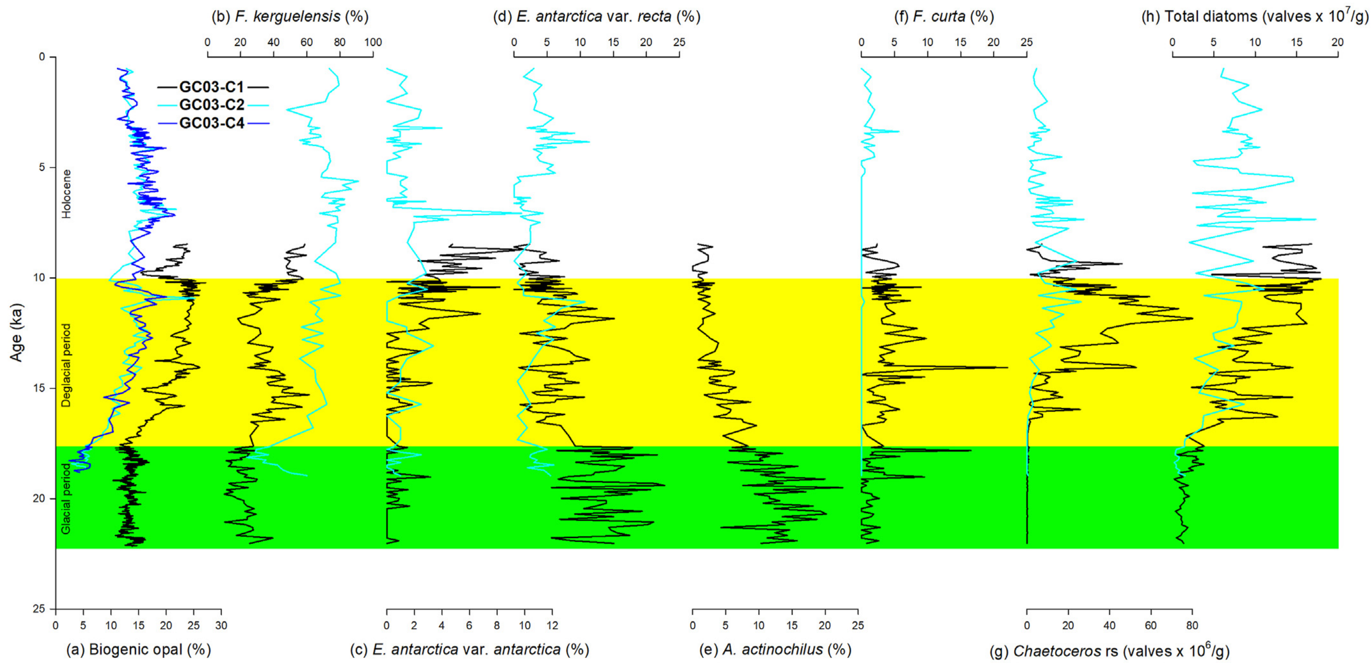

Fig. 4. Downcore profiles of (a) biogenic opal concentration, relative abundance of (b) *F. kerguelensis*, (c) *E. antarctica* var. *antarctica*, (d) *E. antarctica* var. *recta*, (e) *A. actinochilus*, and (f) *F. curta*, (g) *Chaetoceros* resting spores, and (h) total diatoms of cores GC03-C1 (black), -C2 (cyan), and -C4 (blue). Diatom records for GC03-C1 are from Bak et al. (2010) and for GC03-C2 are from Bak et al. (2014), except for *Chaetoceros* resting spores in GC03-C2 (this study).

since the last glacial period (Fig. 2). As *F. kerguelensis* was reported as an important contributor to carbon transfer to depth (Grigorov et al., 2014), *F. kerguelensis*-dominant diatom assemblage of all cores can cause good correlations between biogenic opal and TOC. This is in agreement with previous studies that have identified high diatom production in the Southern Ocean south of the PF (Honjo et al., 2000). As C/N ratios are lower in marine organic matter relative to terrestrial organic matter (Lamb et al., 2006Lamb et al., 2006 and references therein), the lower C/N ratios after 17.6 ka may be indicative of high diatom organic matter (Fig. 2).

The biogenic opal and diatom abundance records indicate lower surface water productivity during the glacial period (before 17.6 ka) relative to the Holocene (Figs. 2 and 4). The deglacial period is characterized by decreases in sea ice diatoms (*A. actinochilus; Armand et al., 2005*) and the glacial dominant species (*E. antarctica* var. *recta*) and increases in both open ocean species (*F. kerguelensis*) and *Chaetoceros* resting spores, and total diatom valves (Bak et al., 2010, 2014, Fig. 4). The sea ice diatom *F. curta* did not show a clear change during the deglacial period; however, the decreased abundances of sea ice species *A. actinochilus* and cold water mass species *E. antarctica* var. *recta* (Leventer et al., 2002Leventer et al., 2002) imply reduced sea ice during the deglaciation. These findings indicate increased surface water productivity in response to sea ice retreat and an increased influence of the ACC in the Scotia Sea. The dominance of *F. kerguelensis* in other sediment cores PS67/197-1 and PS67/219-1 in the Scotia Sea also suggests increased opal production under open ocean conditions during interglacial periods (Xiao et al., 2016). Thus, it has been suggested that an increase in surface water productivity during interglacial periods is related to retreat of sea ice which inhibits light availability.

As the SBACC is related to the winter sea ice extent (Xiao et al., 2016 and references therein), the sea ice retreat during the deglaciation is likely accompanied by the increasing influence of the ACC on the core site (Roberts et al., 2017). However, despite the importance of the ACC on surface water production, past changes in the influence of the ACC in the Scotia Sea have not yet been considered in terms of surface water productivity. Bulk $\delta^{15}N$ has been used as a nitrate utilization proxy (Francois et al., 1992; Altabet and Francois, 1994), including in the western AP (Kim et al., 2018b). As Schubert and Calvert (2001)Schubert and Calvert, 2001 reported the presence of inorganic nitrogen (IN) in the polar region (Arctic), we compared the $\delta^{15}N_{acid}$ and the bulk $\delta^{15}N$ trend to determine the isotopic influence of IN in GC03-C1 (e.g., Nie et al., 2014). Since the trends are almost identical with r^2 of 0.94 (Fig. 2), we conclude that the influence of IN is negligible; consequently, $\delta^{15}N_{acid}$ in GC03-C1 and bulk $\delta^{15}N$ in GC03-C2 can be compared without any analytical offset. Despite the ~1‰ difference between $\delta^{15}N_{acid}$ in GC03-C1 (lower) and bulk $\delta^{15}N$ in GC03-C2 (higher), the two records indicate higher nutrient utilization during the last glacial period relative to the Holocene (Fig. 2). If surface water productivity is predominantly controlled by changes in sea ice extent, we expect to observe enhanced nutrient utilization at the core sites due to increased light availability in response to sea ice retreat. However, nitrate utilization decreased despite increased surface water productivity and reduced sea ice influence (Fig. 2). To explain increased export and diatom production in the surface water with decreased nutrient utilization, the total amount of nutrient supplied should be increased. Since this is typical of a place characterized by enhanced nutrient supply from sub-surface water (e.g., Brzezinski et al., 2002; Brunelle et al., 2010; Studer et al., 2015; Kim et al., 2018b), increased surface water productivity in the Scotia Sea since the deglaciation is likely related to increased sub-surface nutrient supply by a strengthening ACC in response to sea ice retreat. This is consistent that a southward shift of all fronts during deglacial period occurred with enhancing ACC in the Drake Passage (Roberts et al., 2017). Thus, our results suggest that nutrient availability associated with the ACC-sea ice balance was the dominant control on surface water productivity in the Scotia Sea during the deglaciation.

Bulk $\delta^{15}N$ values—and therefore nutrient utilization—continued

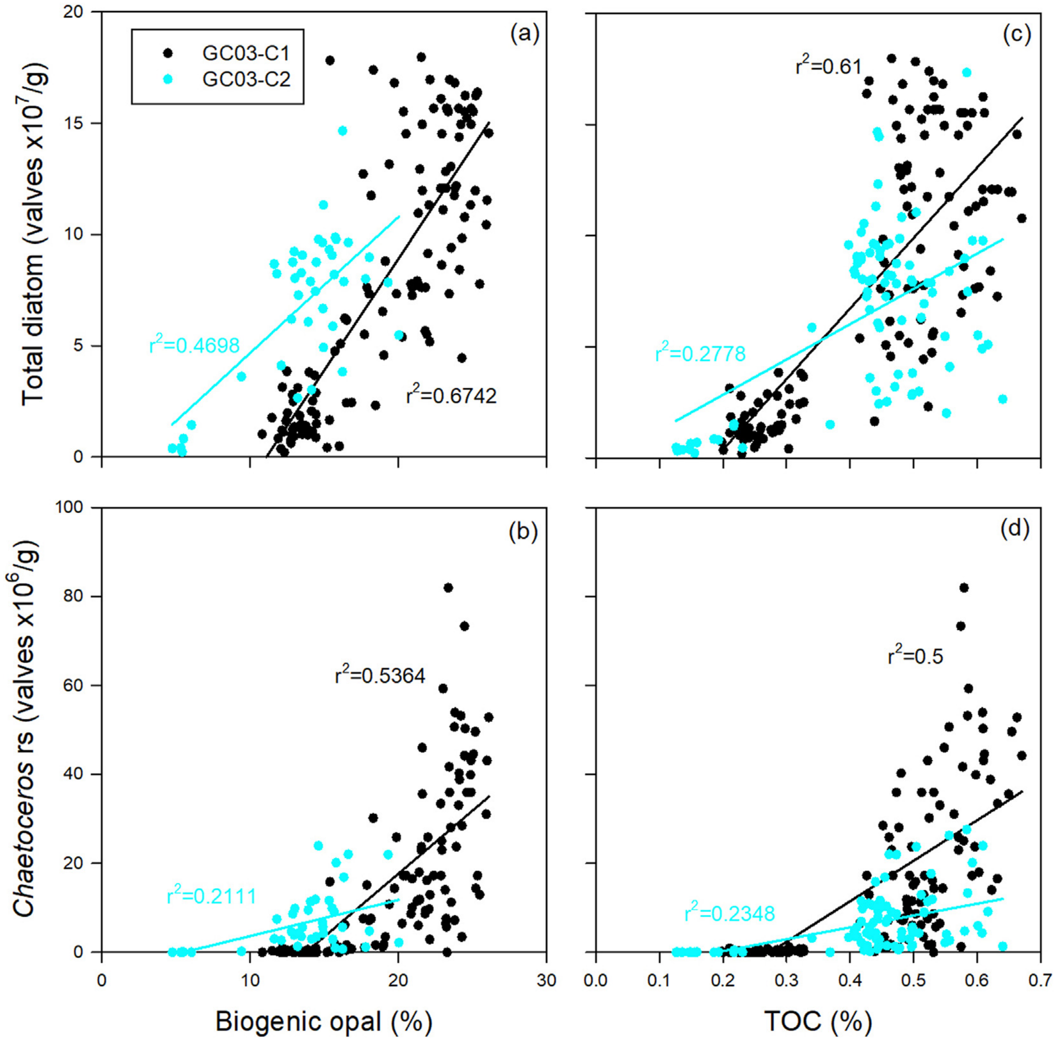

Fig. 5. Correlations of biogenic opal concentration with (a) total diatom abundance and (b) *Chaetoceros* resting spores and of TOC concentration with (c) total diatom abundance and (d) *Chaetoceros* resting spores for GC03-C1 (black) and GC03-C2 (cyan). (For interpretation of the references to colour in this figure legend, the reader is referred to the Web version of this article.)

to decrease until the late Holocene (Fig. 2). According to the trends in biogenic opal and diatom abundance, diatom production at cores GC03-C2 and GC03-C4 began to decrease gradually after 7 ka (Figs. 2 and 4); this suggests a change in the relationship between diatom production and nutrient utilization after 7 ka (Figs. 2 and 6). We observed a negative and positive relationship between biogenic opal production and nutrient utilization before and after 7 ka, respectively (Fig. 6). The positive relationship after 7 ka may be due to a deepening of the mixed layer depth (MLD) and/or increasing sea ice extent. The diatom assemblage record for GC03-C2 after 7 ka showed low/insignificant variability of sea ice species (including *F. curta*) and an increasing abundance of the cold water species *E. antarctica* var. *recta* (Fig. 4). McCave et al. (2014) reported a faster ACC during the Holocene relative to the glacial period in the sea ice zone south of 56°S. A strengthened ACC at the core site would have caused a deepening of the MLD (i.e., cooling in the surface ocean). A deepening MLD is also supported by the decreased abundance of *Chaetoceros* resting spores in GC03-C2 since 7 ka (Fig. 4), which are indicative of high production and melt water stratification (Leventer, 1991; Leventer et al., 1996; Crosta et al., 2004). The lower export production per diatom production after 7 ka also supports a deepening of the MLD (Fig. 6a).

TOC concentrations are similar between all cores, but biogenic opal concentrations are significantly higher in GC03-C1 (Fig. 2). Diatom Si/NO_3^- uptake ratios are dependent on Fe availability, with high (low) ratios coinciding with low (high) Fe concentrations (Hutchins and Bruland, 1998; Hutchins et al., 2002). Fe concentrations decrease with increasing distance from the Antarctic continent in the western AP (De Jong et al., 2015). The geomorphology of our study region causes the fronts to merge at our core sites, our results therefore show that the small latitudinal differences between the core sites can result in significant differences in Fe concentrations. However, due to the wide frontal distribution in the central to eastern Scotia Sea, core records located in this region showed no decreasing trends in biogenic opal (e.g., Sprenk et al., 2013; Xiao et al., 2016).

Bulk $\delta^{15}N$ is influenced by both nutrient utilization and changes in diatom assemblage (Needoba et al., 2003; Horn et al., 2011). It is difficult to identify strong correlations between diatom assemblage and bulk $\delta^{15}N$ (or $\delta^{15}N_{acid}$) variability in cores GC03-C1 and GC03-C2 (Bak et al., 2010, 2014) (Fig. 2); this suggests that bulk $\delta^{15}N$ values more likely reflect changes in diatom nutrient utilization in Scotia Sea surface water. Despite minor offsets, the $\delta^{15}N$ values of pennate, central, and total diatoms were found to co-vary (Studer

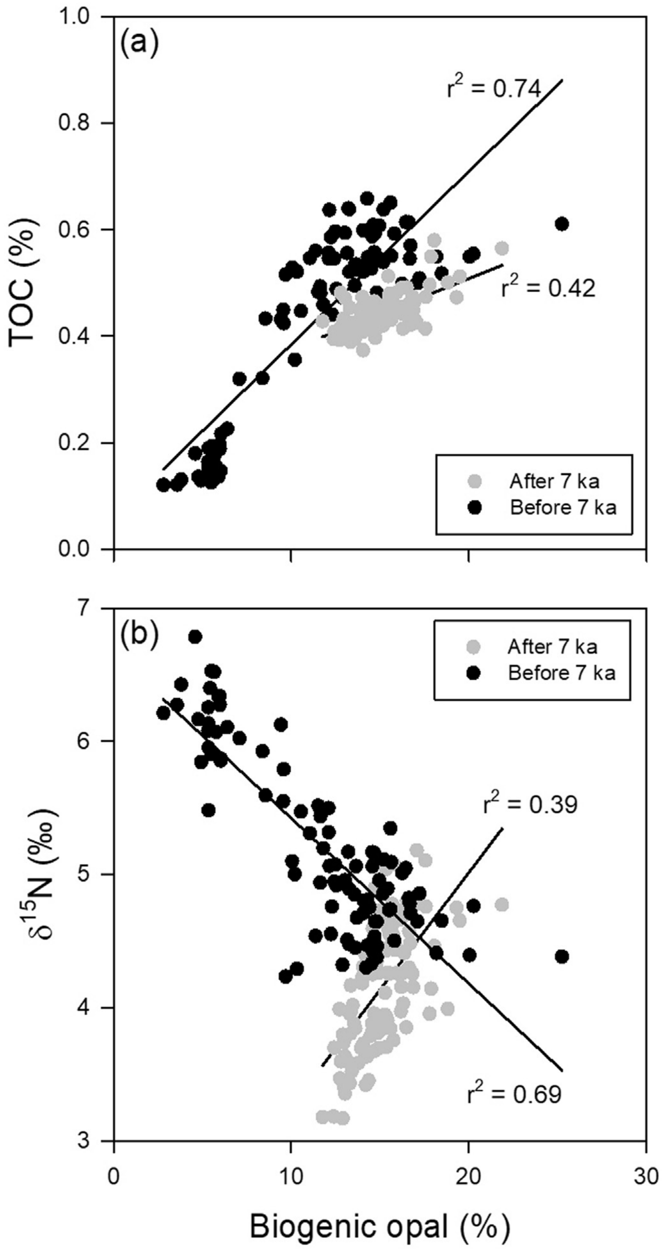

Fig. 6. Correlations of biogenic opal concentration with (a) TOC concentration and (b) bulk $\delta^{15}N$ from core GC03-C2 before (black) and after 7 ka (gray).

et al., 2015). In addition, bulk $\delta^{15}N$ was found to reflect as nutrient utilization in the western AP (Kim et al., 2018b). Sedimentary records of diatom assemblages reflect the diatoms that are preserved rather than diatoms that lived in the surface water (Crosta and Koç, 2007); therefore, it is more likely that $\delta^{15}N$ values reflect the total nutrient utilization of phytoplankton—dominated by diatom production—in the surface water.

6.2. Iceberg calving activity since the last glacial period

Down-core coarse-grain abundances have been used as an indicator for IRD in the Southern Ocean (Diekmann et al., 2000; Weber et al., 2012, 2014). Weber et al. (2014) reported that increased IRD during the last deglacial period in the Scotia Sea is indicative of large-scale iceberg calving during ice sheet/shelf retreat. Grains >1 mm were observed throughout all cores; however, higher abundance was observed during the last deglaciation (17.6–9 ka) in the southern Scotia Sea (Fig. 3). This suggests continued iceberg calving since the last glacial period in the southern Scotia Sea, with highest activity during the deglaciation. The high abundance of *Chaetoceros* resting spores—indicative of high productivity and melt water stratification (Leventer 1991; Leventer et al., 1996; Crosta et al., 2004)—also indicates large-scale ice melting and the rapid retreat of the AP and/or Weddell Sea ice sheets in response to deglacial warming (Fig. 4). We observed highest abundance of grains >1 mm in all three cores from 16 to 14.5 ka and 11.1–9 ka coinciding with increases in the relative abundance of open ocean diatoms such as *F. kerguelensis* at GC03-C1 (Figs. 3 and 4). These time periods correspond to previously reported intervals of high IRD flux to the Scotia Sea (Weber et al., 2014), indicating the potential contribution of ice sheet/shelf melting to global sea level rise. Because clay fraction of GC03-C2 and GC03-C4 showed relatively high values (*ca.* 15%) between 17.6 and 12.5 ka (Fig. 3), it can be interpreted that clay supply increased during ice sheet/shelf melting and retreating. Therefore, our results indicate rapid reduction of ice sheets/shelves in the Weddell Sea and the western AP in response to oceanic forcing from sea ice retreat and atmospheric warming (Fig. 3i; Jouzel et al., 2007).

A wide range of grain size—including coarse grains (>1 mm)—can act as an indicator for IRD (Andrews, 2000; Jonkers et al., 2012, 2015; McCave and Andrews, 2019). For example, analysis of sediment grain size distribution in Svalbard icebergs showed that the grains were predominantly ranged from coarse silt to fine sand (Jonkers et al., 2015). Studies have identified strong correlations between sediment core MS records in the Scotia Sea and the EDML ice core dust record (e.g., Pugh et al., 2009; Weber et al., 2012; Xiao et al., 2016; Kim et al., 2018a; Shin et al., 2020). However, proposed mechanisms were different. Kim et al. (2018a) found good correlations between the MS values and grain size (particularly with coarse silt to fine sand-sized grains of 16–250 μm) from southern Scotia Sea cores including GC03-C2 and GC03-C4, and they interpreted that the coarse silt to fine sand-sized grains having high MS values were delivered as IRD during the glacial period. Although biogenic magnetite was suggested to control MS values in the sub-Antarctic Indian Ocean which is far from the Scotia Sea (Yamazaki and Ikehara, 2012), Shin et al. (2020) reported that coarse silt to fine sand grains having high MS values were delivered as IRD during the glacial period based on magnetic properties. The strong correlations between MS, MGS, and the sand fraction in all cores suggest that high MS values during glacial periods are related to grain size, particularly the coarse silt to fine sand fraction (Figs. 3 and 7). Thus, the high MS variation of all cores implies that the iceberg calving was active during the glacial period and decreased from 17.6 ka.

Intriguingly, grain size distribution of IRD in sediments are different; with coarse silt to fine sand dominant size during the glacial period vs with more grains >1 mm during the deglacial period (Fig. 3). If IRD source material is assumed same including grain size distribution and provenance between two different time intervals, the discrepancy must be related to depositional process. A high flow speed can cause reduced deposition rate of fine fraction, but sand sized grains are considered difficult to be moved. MS values/g and magnetic properties of sand and coarse silt fractions vary between the glacial and deglacial period in GC03-C1 (Shin et al., 2020). The relative abundance of sand and coarse silt fractions can vary, but similar values are expected if IRD source material is same. Thus, the different characteristics of IRD between the glacial and the deglacial period indicate that IRD source characteristics are different.

Because the study area is located at the extension of Iceberg

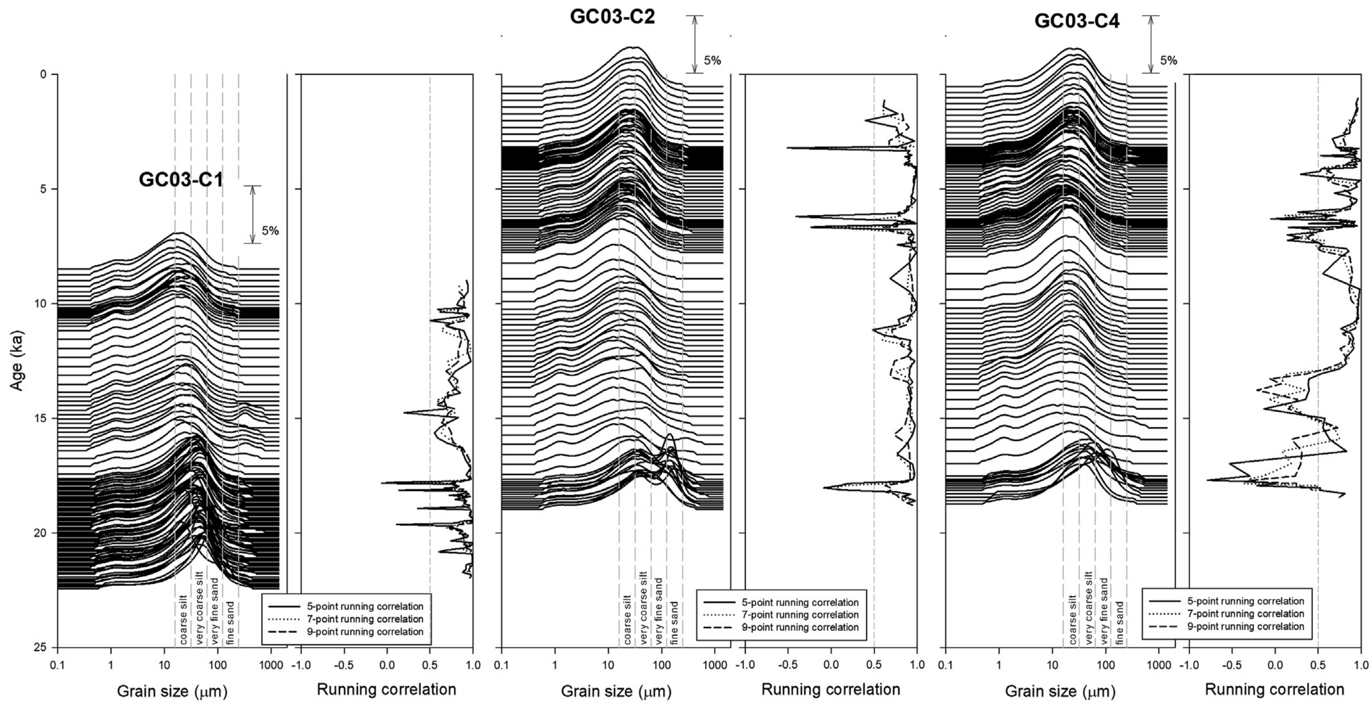

Fig. 7. Downcore profiles of grain size distribution and the running 5-, 7-, and 9-point correlation between the SS MGS and SS% for GC03-C1, -C2, and -C4. (Very) coarse silt and (very) fine sand sizes are shown by long dashed lines. R value of 0.5 is shown as short dashed lines.

Alley (Fig. 1), the study area receives a mixture of icebergs from all around the Antarctica. This means that it is difficult to identify the IRD provenance in our cores. There is a possibility that the study site received IRDs originating from the western part of AP Ice sheet/shelf during the glacial period when ice sheet/shelf reached close to the shelf break (Bentley et al., 2014). Nevertheless, it is difficult to confine its source region in this study due to lack of detailed information on properties of potential source regions. Of note is that the size characteristics of IRD during glacial and deglacial periods are different in the Scotia Sea. Thus, the IRD estimation by the coarse fraction can lead to underestimation of iceberg calving particularly during glacial periods in response to ice-sheet expansion in the Scotia Sea (Jonkers et al., 2015; Kim et al., 2018a). Although smaller sizes (125 or 150 μm) were applied for determining IRD in other regions of the Antarctica (e.g., Passchier, 2011; Patterson et al., 2014), our results still suggest potential underestimation of iceberg calving during glacial periods. To fully understand iceberg calving history in the Antarctica, further studies are required.

6.3. Bottom current intensity changes

The SS MGS is commonly used to reconstruct bottom current intensity (McCave et al., 1995, 2017; McCave and Andrews, 2019) and bottom current speed (e.g., Bianchi and McCave, 1999; Boessenkool et al., 2007; Jonkers et al., 2015; Wu et al., 2018). IRD deposition has the potential to influence the SS MGS (Jonkers et al., 2015), as IRD is not only limited to the coarse-grain size fraction (e.g., Dowdeswell and Dowdeswell, 1989; Andrews, 2000; Jonkers et al., 2012, 2015; Kim et al., 2018a). IRD input can influence MGS of SS such that it does not reflect flow speed (Jonkers et al., 2015). If sediments are predominantly current-sorted, McCave and Andrews (2019) argue that SS MGS records can provide reliable paleo-current data, despite the input of IRD. Thus, it is necessary to be assessed if the SS MGS during the glacial period can be used as an indicator for paleo current intensity.

Well sorted surface sediments by the bottom current showed a good correlation between the SS MGS and SS% (McCave and Andrews, 2019). Although the running downcore correlations (5 to 9-point) in GC03-C4 showed <0.5 before 12.5 ka, they were generally >0.5 in GC03-C1 and GC03-C2, except for some short intervals (Fig. 7). According to McCave and Andrews (2019), this indicates that the SS MGS can be used as a paleo-current speed indicator in this study regardless of IRD influence.

All three cores are divided into three intervals; the glacial period with high MS values, deglacial period, and the Holocene with low MS values, thus linear regressions were calculated by each period (Fig. 8). The relationship between the SS MGS and SS% at GC03-C1 clearly suggests that SS is well current-sorted for all time intervals, but with different slopes (Fig. 8a). In contrast, the relationships at GC03-C2 and GC03-C4 showed relatively high to low correlations for the glacial and deglacial periods (Fig. 8). Nevertheless, the relationships in all cores for the Holocene showed strong correlations (Fig. 8). This is probably related to characteristics of input sediments and this clearly suggests that changes in SS MGS needs to be discussed by the different time periods.

Based on the SS MGS changes between the Holocene and the last glacial period, the ACC bottom current (i.e., the intensity of the ACC) was studied in the Drake Passage and the Scotia Sea (McCave et al., 2014). SS MGS is coarser during the glacial period than the Holocene (Fig. 3). Coarser SS MGS during the LGM was also found from the eastern Scotia Sea core located near the SBACC (McCave et al., 2014). If the influencing bottom current was the ACC during the glacial period, it means that the ACC was enhanced during the glacial period under more extensive sea ice and northward migrated fronts. Thus, the bottom current during the glacial period in the study area was not related to the ACC. Drift sediments are well developed in the AP margin in association with southwestward flowing bottom current (Barker and Camerlenghi, 2002), and Lucchi et al. (2002) and Lucchi and Rebesco (2007) reported

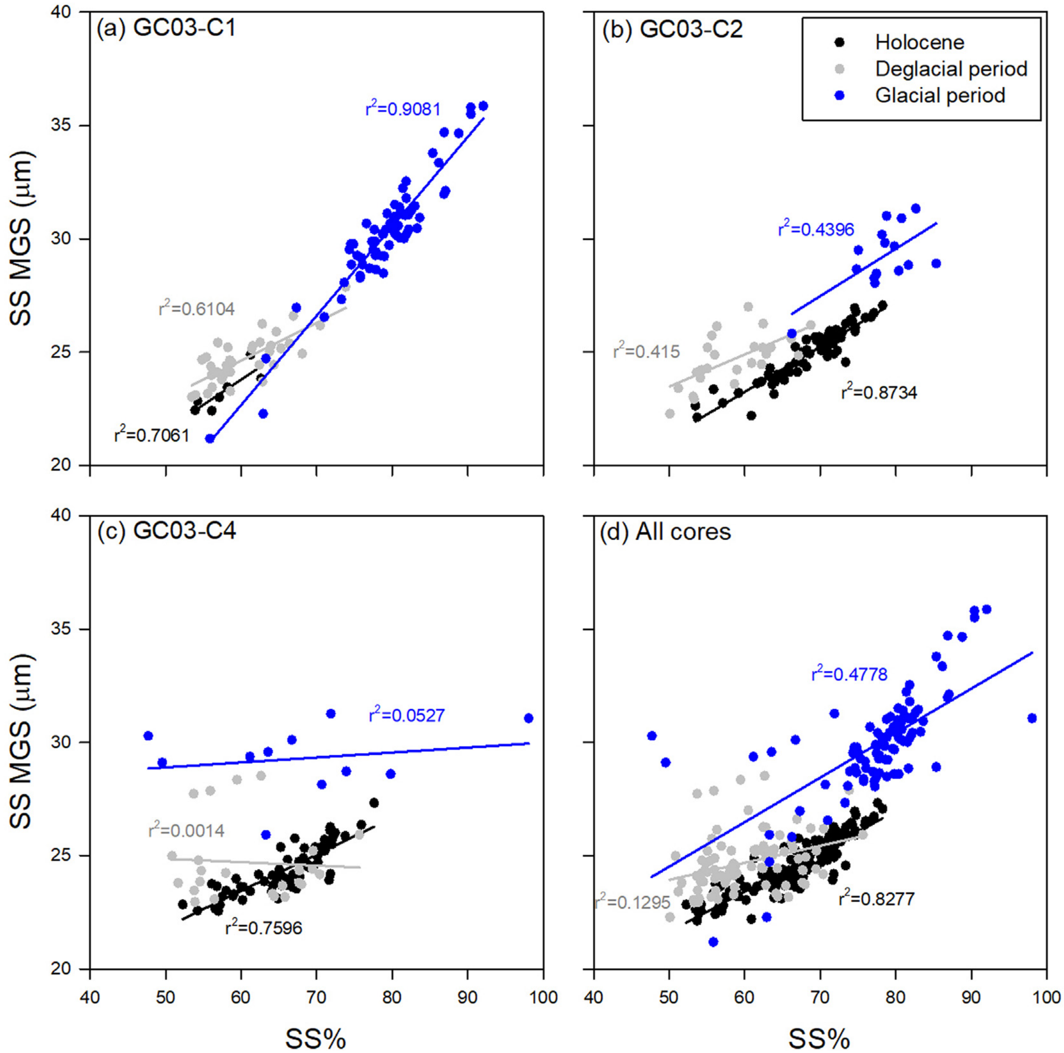

Fig. 8. Correlations of the SS MGS and SS% for (a) GC03-C1, (b) GC03-C2, (c) GC03-C4, (d) and all three cores for the last glacial period (blue), the deglacial period (gray), and the Holocene (black). (For interpretation of the references to colour in this figure legend, the reader is referred to the Web version of this article.)

contourite deposition during glacial periods indicating the presence of southwestward flowing bottom current. Considering the direction of the bottom current and the location of our cores, the study site was most likely influenced by the southwestward flowing bottom current during the glacial period under more extensive sea ice and northward migrated fronts conditions accompanying with weakened ACC influence on the site. As the relationships between the SS MGS and SS% are different between the Holocene and the glacial period (Fig. 8), paleo-current intensity comparison between the Holocene and the glacial period by SS MGS need a caution. Nevertheless, ~10 μm difference suggests that the bottom current speed was faster during the glacial period.

All cores showed a continuous decrease in the SS MGS during the deglacial period (Fig. 3) and good correlations between the SS MGS and SS% are found in GC03-C1 and GC03-C2 during the deglacial period (Fig. 8). This indicates that the bottom current intensity continuously decreased with climate warming accompanying with southward migration of fronts. Thus, the southwestward flowing bottom current is thought to be weakened probably due to southward migration.

The SS MGS started to increase from 7 ka in GC03-C2 and GC03-C4 (Fig. 3). This implies a strengthening bottom current from the early to the late Holocene in the southern Scotia Sea. Since our core site is close to the SBACC in modern days (Orsi et al., 1995), the dominant bottom current must be the ACC during the Holocene. The deepening of the MLD after 7 ka also supports increased influence of the ACC. Thus, the increasing SS MGS from 7 ka suggests a strengthening ACC. In addition, the enhancing ACC at our sites indicates is related to ongoing southward migration.

6.4. Ocean-cryosphere interactions since the last glacial period

The schematic environmental model for the last glacial period was presented in Fig. 9a. The last glacial period was characterized by extensive sea ice and an advanced ice shelf (Gersonde et al., 2005; Bak et al., 2010, 2014; Collins et al., 2012; Bentley et al., 2014; Xiao et al., 2016). All fronts including the SBACC therefore shifted northward during the last glacial period, which reduced the influence of the ACC in the study site. The diatom production decreased accompanying with enhanced nutrient utilization, indicating increased surface water stratification (Figs. 2 and 4). Iceberg calving was active and coarse silt to fine sand grains were dominantly supplied as IRD with less grains >1 mm. Good correlations between the SS MGS and SS% in GC03-C1 and GC03-C2 indicate that

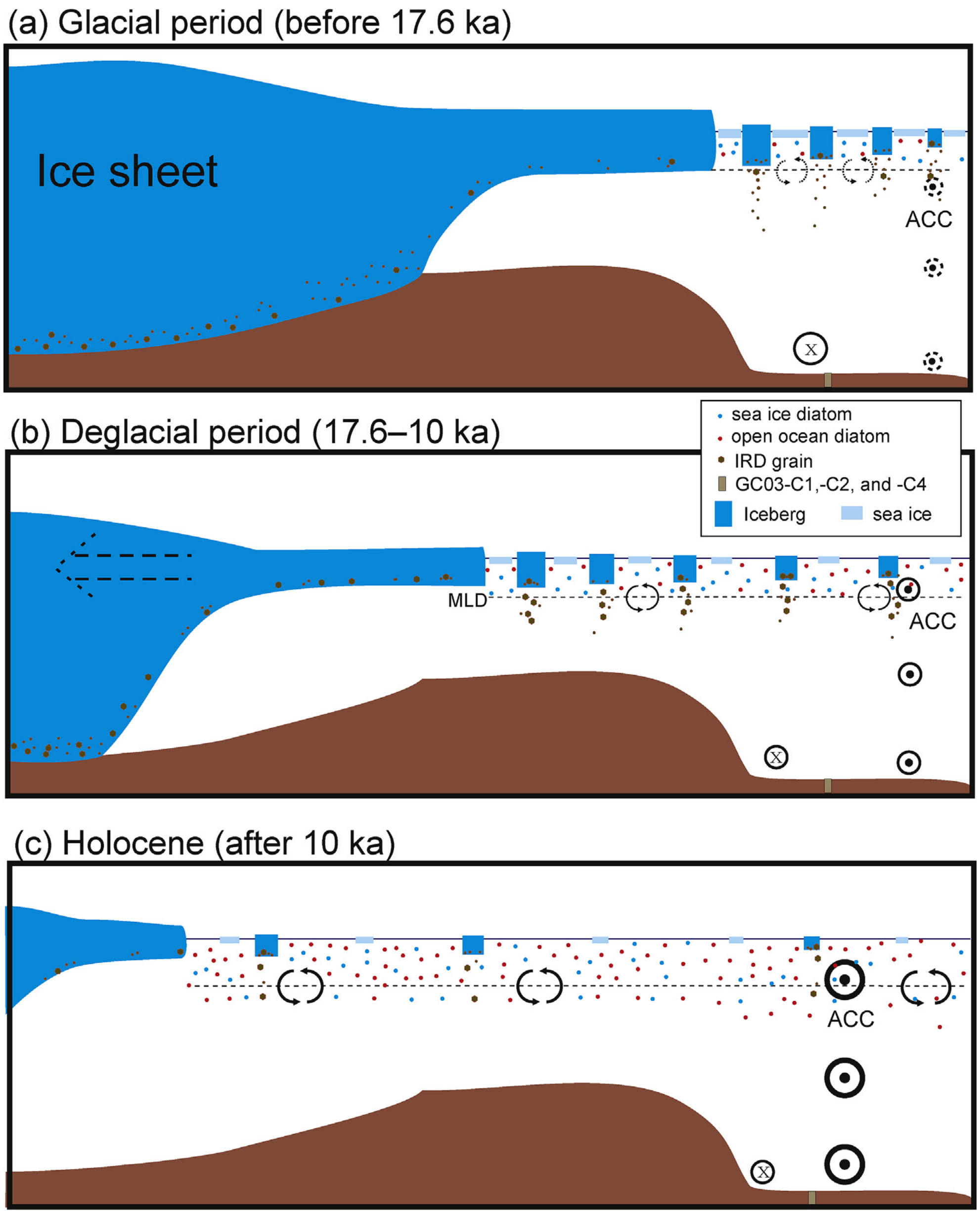

Fig. 9. Paleoceanographic models of (a) the glacial period (before 17.6 ka), (b) the deglacial period (17.6–10 ka), and (c) the Holocene (after 10 ka) in the Southern Ocean off Elephant Island. MLD is the mixed layer depth.

the sediments are sorted by the southwestward flowing bottom current. Southwestward flowing bottom current was enhanced under weakened ACC influence contemporaneously with northward migration of fronts.

The schematic environmental model for the deglacial period was presented in Fig. 9b. Sea ice retreat after 17.6 ka created open ocean conditions in the southern Scotia Sea (Bak et al., 2010, 2014; Xiao et al., 2016); this caused an increase in surface water productivity. Because nutrient utilization was not increased accompanying with increased light penetration, more nutrients were supplied from the subsurface water in response to the southward migration of fronts including the SBACC during the deglaciation. Iceberg calving also occurred during the deglaciation contemporaneously with rapid ice shelf/sheet break; however, grains >1 mm were abundantly deposited (Fig. 9b). Good correlations between the SS MGS and SS% in GC03-C1 and GC03-C2 indicate that the sediments are sorted by the southwestward flowing bottom current. The southwestward flowing bottom current became weak contemporaneously with climate warming.

The schematic environmental model for the Holocene was presented in Fig. 9c. Surface water production started to decrease at 7 ka with a shift of the relationship between surface water production and nutrient utilization from being negative to positive. Decreases in surface water production and nutrient utilization and an increase in cold water diatom species after 7 ka indicate further deepening of the MLD, deeper than euphotic zone, associated with the enhanced ACC. High correlations between the SS MGS and SS% indicate that the SS is sorted by bottom current. The SS MGS continued to increase after 7 ka, indicating the increased ACC bottom current. This means that southward migration of the ACC and other fronts persisted from 7 ka.

7. Conclusions

We reconstructed the past variability of surface water productivity, nutrient utilization, bottom current intensity, and iceberg calving since the last glacial period using three sediment cores (GC03-C1, -C2, and -C4) in the Southern Ocean off Elephant Island. During the last deglaciation, surface water productivity increased with decreased nutrient utilization as sea ice retreats, indicating enhanced subsurface nutrient supply in response to an intensified surface current. Diatom production decreased along with decreased nutrient utilization from 7 ka due to deeper MLD than euphotic zone derived by enhancing ACC with further southward migration.

Running downcore correlations of the SS MGS and SS% of all cores indicate that sediments are sorted by bottom currents regardless of IRD influence. However, the slopes were different among different time intervals. Bottom current speed decreased during the deglacial period with southward migration of the ACC and fronts, implying that the dominant bottom current was most likely southwestward flowing bottom current. The influence of the ACC started to increase from 7 ka with further southward migration of the ACC and fronts.

Coarse silt to fine sand sized grains with sparse grains >1 mm were the dominant IRD grain size in sediments of the glacial period. In contrast, during the deglacial period, grains >1 mm occurred abundantly, which indicates large-scale ice melting and the rapid retreat of ice sheets during the deglaciation. Although the source IRD regions for the glacial and deglacial periods are not sure, the different grain size characteristics of IRD in sediments are thought to reflect different IRD source characteristics. Our multi-proxy records show that the sedimentary processes in the Southern Ocean off Elephant Island were significantly linked to the dynamics of the ocean–cryosphere system.

Credit author statement

Sunghan Kim: Conceptualization, Methodology, Writing – Original Draft and Review & Editing, **Kyu-Cheul Yoo**: Writing – Review & Editing, Supervision, Resources, Investigation, **Jae Il Lee**: Investigation, Writing – Review & Editing, **Youn Ho Roh**: Data Curation (IRD counting), **Young-Suk Bak**: Data Curation (Diatom), Validation (Diatom part), **In-Kwon Um**: Data Curation (Grain size analysis), **Min Kyung Lee**: Writing – Review & Editing, **Ho Il Yoon** Project administration.

Declaration of competing interest

The authors declare that they have no known competing financial interests or personal relationships that could have appeared to influence the work reported in this paper.

Acknowledgements

We would like to thank the crew and scientific party of the R/V *Yuzhmorgeologiya* for their support during the onboard gravity coring. We would like to thank the KOPRI laboratory members for their assistance with experimental measurements. We appreciate the handling editor (Dr. Antje Voelker) and three anonymous reviewers for their important and constructive comments to improve data interpretation and manuscript structure. This research was supported by the KOPRI project (PE20180).

Appendix A. Supplementary data

Supplementary data to this article can be found online at https://doi.org/10.1016/j.quascirev.2020.106563.

References

Altabet, M.A., Francois, R., 1994. Sedimentary nitrogen isotopic ratio as a recorder for surface ocean nitrate utilization. Global Biogeochem. Cycles 8, 103–116.

Anderson, J.B., Andrew, J.T., 1999. Radiocarbon constraints on ice sheet advance and retreat in the Weddell Sea, Antarctica. Geology 27, 179–182.

Andrews, J., 2000. Icebergs and iceberg rafted detritus (IRD) in the North Atlantic: facts and assumptions. Oceangraphy 13, 100–108.

Armand, L.K., Crosta, X., Romero, O., Pichon, J.-J., 2005. The biogeography of major diatom taxa in Southern Ocean sediments: 1. Sea ice related species. Palaeogeogr. Palaeoclimatol. Palaeoecol. 223, 93–126.

Bak, Y.S., Lee, J.D., Yoon, H.I., Yoo, K.C., Lee, S.J., 2010. Holocene paleo-climate change in the area around Elephant Island, Antarctica: evidence from the diatom record. J. Geol. Soc. Korea 46, 111–117 (in Korean with English abstract).

Bak, Y.S., Yoo, K.C., Yoon, H.I., 2014. Late quaternary climate changes around the Elephant Islands, antarctic Peninsula. Geosci. J. 18, 495–501. https://doi.org/10.1007/s12303-014-0011-0.

Barker, P.F., Camerlenghi, A., 2002. Glacial history of the antarctic Peninsula from Pacific margin sediments. In: Barker, P.F., Camerlenghi, A., Acton, G.D., Ramsay, A.T.S. (Eds.), Proc. ODP, Sci. Results, 178 [Online]. http://www-odp.tamu.edu/publications/178_SR/synth/synth.htm.

Bentley, M.J., Cofaigh, C.Ó., Anderson, J.B., Conway, H., Davies, B., Graham, A.G.C., Hillenbrand, C.-D., Hodgson, D.A., Jamieson, S.S.R., Larter, R.D., Mackintosh, A., Smith, J.A., Verleyen, E., Ackert, R.P., Bart, P.J., Berg, S., Brunstein, D., Canals, M., Colhoun, E.A., Crosta, X., Dickens, W.A., Domack, E., Dowdeswell, J.A., Dunbar, R., Ehrmann, W., Evans, J., Favier, V., Fink, D., Fogwill, C.J., Glasser, N.F., Gohl, K., Golledge, N.R., Goodwin, I., Gore, D.B., Greenwood, S.L., Hall, B.L., Hall, K., Hedding, D.W., Hein, A.S., Hocking, E.P., Jakobsson, M., Johnson, J.S., Jomelli, V., Jones, R.S., Klages, J.P., Kristoffersen, Y., Kuhn, G., Leventer, A., Licht, K., Lilly, K., Lindow, J., Livingstone, S.J., Massé, G., McGlone, M.S., McKay, R.M., Melles, M., Miura, H., Mulvaney, R., Nel, W., Nitsche, F.O., O'Brien, P.E., Post, A.L., Roberts, S.J., Saunders, K.M., Selkirk, P.M., Simms, A.R., Spiegel, C., Stolldorf, T.D., Sugden, D.E., van der Putten, N., van Ommen, T., Verfaillie, D., Vyverman, W., Wagner, B., White, D.A., Witus, A.E., Zwartz, D., the RAISED Consortium, 2014. A community-based geological reconstruction of antarctic ice sheet deglaciation since the last glacial maximum. Quat. Sci. Rev. 100, 1–9. https://doi.org/10.1016/j.quascirev.2014.06.025.

Bianchi, G.G., McCave, I.N., 1999. Holocene periodicity in North Atlantic climate and deep-ocean flow south of Iceland. Nature 397, 515–517.

Boessenkool, K.P., Hall, I.R., Elderfield, H., Yashayaev, I., 2007. North Atlantic climate and deep-ocean flow speed changes during the last 230 years. Geophys. Res. Lett. L13614 https://doi.org/10.1029/2007GL030285.

Brunelle, B.G., Sigman, D.M., Jaccard, S.L., Keigwin, L.D., Plessen, B., Schettler, G., Cook, M.S., Haug, G.H., 2010. Glacial/interglacial changes in nutrient supply and stratification in the western subarctic North Pacific since the penultimate glacial maximum. Quat. Sci. Rev. 29, 2579–2590.

Brzezinski, M.A., Pride, C.J., Franck, V.M., Sigman, D.M., Sarmiento, J.L., Matsumoto, K., Gruber, N., Rau, G.H., Coale, K.H., 2002. A switch from $Si(OH)_4$ to NO_3^- depletion in the glacial Southern Ocean. Geophys. Res. Lett. 29 https://doi.org/10.1029/2001GL014349, 5-1–5-4.

Burckle, L.H., Burak, R.W., 1988. Fluctuations in Late Quaternary diatom abundances: stratigraphic and paleoclimatic implications from subantarctic deep sea cores. Palaeogeogr. Palaeoclimatol. Palaeoecol. 67, 147–156.

Cárdenas, P., Lange, C.B., Vernet, M., Esper, O., Srain, B., Vorrath, M.E., Ehrhardt, S., Müller, J., Kuhn, G., Arz, H.W., Lembke-Jene, L., Lamy, F., 2019. Biogeochemical proxies and diatoms in surface sediments across the Drake Passage reflect oceanic domains and frontal systems in the region. Prog. Oceanogr. 174, 72–88. https://doi.org/10.1016/j.pocean.2018.10.004.

Collins, L.G., Pike, J., Allen, C.S., Hodgson, D.A., 2012. High-resolution reconstruction of southwest Atlantic sea-ice and its role in the carbon cycle during marine isotope stages 3 and 2. Paleoceanography 27, PA3217.

Crosta, X., Koç, N., 2007. Chapter eight diatoms: from micropaleontology to isotope geochemistry. Dev. Mar. Geol. 1, 327–369. https://doi.org/10.1016/S1572-5480(07)01013-5.

Crosta, X., Pichon, J.J., Labracherie, M., 1997. Distribution of *Chaetoceros* resting spores in modern peri-Antarctic sediments. Mar. Micropaleontol. 29, 283–299.

Crosta, X., Sturm, A., Armand, L., Pichon, J.J., 2004. Late Quaternary sea ice history in the Indian sector of the Southern Ocean as recorded by diatom assemblages. Mar. Micropaleontol. 50, 209–223. https://doi.org/10.1016/S0377-8398(03)00072-0.

De Jong, J.T.M., Stammerjohn, S.E., Ackley, S.F., Tison, J.L., Mattielli, N., Schoemann, V., 2015. Sources and fluxes of dissolved iron in the Bellingshausen Sea (West Antarctica): the importance of sea ice, icebergs and the continental margin. Mar. Chem. 177, 518–535. https://doi.org/10.1016/j.marchem.2015.08.004.

DeMaster, D.J., 1981. The supply and accumulation of silica in the marine environment. Geochem. Cosmochim. Acta 5, 1715–1732.

Diekmann, B., 2007. Sedimentary patterns in the late quaternary Southern Ocean. Deep-Sea Res. II 54, 2350–2366.

Diekmann, B., Kuhn, G., Rachold, V., Abelmann, A., Brathauer, U., Fütterer, D.K., Gersonde, R., Grobe, H., 2000. Terrigenous sediment supply in the Scotia Sea (Southern Ocean): response to late quaternary ice dynamics in patagonia and

on the antarctic Peninsula. Palaeogeogr. Palaeoclimatol. Palaeoecol. 162, 357–387.
Donohue, K., Tracey, K., Watts, D., Chidichimo, M., Chereskin, T., 2016. Mean antarctic circumpolar current transport measured in Drake Passage. Geophys. Res. Lett. 43, 11760–11767. https://doi.org/10.1002/2016GL070319.
Dowdeswell, J.A., Dowdeswell, E.K., 1989. Debris in icebergs and rates of glaci-marine sedimentation– Observations from Spitsbergen and a simple model. J. Geol. 97, 221–231.
Folk, R.L., Ward, W.C., 1957. Brazos River bar [Texas]; a study in the significance of grain size parameters. J. Sediment. Res. 27, 3–26.
Francois, R., Altabet, M.A., Burckle, L.H., 1992. Glacial-interglacial changes in surface nitrate utilization in the Indian sector of the Southern Ocean as recorded by sediment δ^{15}N. Paleoceanography 7, 589–606.
Fryxell, G.A., Kendrick, G.A., 1988. Austral spring microalgae across the Weddell Sea ice edge: spatial relationships found along a northward transect during AMERIEZ 83. Deep-Sea Res. 35, 1–20.
Gersonde, R., Crosta, X., Abelmann, A., Armand, L., 2005. Sea-surface temperature and sea ice distribution of the Southern Ocean at the EPILOG Last Glacial Maximum—a circum-Antarctic view based on siliceous microfossil records. Quat. Sci. Rev. 24, 869–896.
Geibert, W., Rutgers van der Loeff, M.M., Usbeck, R., Gersonde, R., Kuhn, G., Seeberg-Elverfeldt, J., 2005. Quantifying the opal belt in the Atlantic and southeast Pacific sector of the Southern Ocean by means of ^{230}Th normalization. Global Biogeochem. Cycles 19, GB4001. https://doi.org/10.1029/2005GB002465.
Gilbert, I.M., Pudsey, C.J., Murray, J.W., 1998. A sediment record of cyclic bottom-current variability from the northwest Weddell Sea. Sediment. Geol. 115, 185–214.
Grigorov, I., Rigual-Hernandez, A.S., Honjo, S., Kemp, A.E.S., Armand, L.K., 2014. Settling fluxes of diatoms to the interior of the Antarctic circumpolar current along 170°W. Deep-Sea Res. I 93, 1–13. https://doi.org/10.1016/j.dsr.2014.07.008.
Hernández-Molina, F.J., Larter, R.D., Rebesco, M., Maldonado, A., 2006. Miocene reversal of bottom water flow along the Pacific Margin of the Antarctic Peninsula: stratigraphic evidence from a contourite sedimentary tail. Mar. Geol. 228, 93–116.
Honjo, S., Francois, R., Manganini, S., Dymond, J., Collier, R., 2000. Particle fluxes to the interior of the Southern Ocean in the western pacific sector along 170°W. Deep-Sea Res. II 47, 3521–3548.
Horn, M.G., Robinson, R.S., Rynearson, T.A., Sigman, D.M., 2011. Nitrogen isotopic relationship between diatom-bound and bulk organic matter of cultured polar diatoms. Paleoceanography 26, PA3208. https://doi.org/10.1029/2010PA002080.
Hutchins, D.A., Bruland, K.W., 1998. Iron-limited diatom growth and Si:N uptake ratios in a coastal upwelling regime. Nature 393, 561–564.
Hutchins, D.A., Hare, C.E., Weaver, R.S., Zhang, Y., Firme, G.F., DiTullio, G.R., Alm, M.B., Riseman, S.F., Maucher, J.M., Geesey, M.E., Trick, C.G., Smith, G.J., Rue, E.L., Conn, J., Bruland, K.W., 2002. Phytoplankton iron limitation in the Humboldt current and Peru upwelling. Limnol. Oceanogr. 47, 997–1011.
Jonkers, L., Prins, M.A., Moros, M., Weltje, G.J., Troelstra, S.R., Brummer, G.-J.A., 2012. Temporal offsets between surface temperature, ice-rafting and bottom flow speed proxies in the glacial (MIS 3) northern North Atlantic. Quat. Sci. Rev. 48, 43–53.
Jonkers, L., Barker, S., Hall, I.R., Prins, M.A., 2015. Correcting for the influence of ice-rafted detritus on grain size-based paleocurrent speed estimates. Paleoceanography 30, 1347–1357. https://doi.org/10.1002/2015PA002830.
Jouzel, J., Masson-Delmotte, V., Cattani, O., Dreyfus, G., Falourd, S., Hoffmann, G., Minster, B., Nouet, J., Barnoloa, J.M., Chappellaz, J., Fischer, H., Gallet, J.C., Johnsen, S., Leuenberger, M., Loulergue, L., Luethi, D., Oerter, H., Parrenin, F., Raisbeck, G., Raynaud, D., Schilt, A., Schwander, J., Selmo, E., Souchez, R., Spahni, R., Stauffer, B., Steffensen, J.P., Stenni, B., Stocker, T.F., Tison, J.L., Werner, M., Wolff, E.W., 2007. Orbital and millennial Antarctic climate variability over the past 800,000 years. Science 317, 793–796.
Kemp, A.E.S., Grigorov, I., Pearce, R.B., Naveira Garabato, A.C., 2010. Migration of the Antarctic Polar Front through the mid-Pleistocene transition: evidence and climatic implications. Quat. Sci. Rev. 29, 1993–2009.
Kim, S., Yoo, K.C., Lee, J.I., Lee, M.K., Kim, K., Yoon, H.I., 2018a. Relationship between magnetic susceptibility and sediment grain size since the last glacial period in the Southern Ocean off the northern Antarctic Peninsula—linkages between the cryosphere and atmospheric circulation. Palaeogeogr. Palaeoclimatol. Palaeoecol. 505, 359–370. https://doi.org/10.1016/J.palaeo.2018.06.016.
Kim, S., Yoo, K.C., Lee, J.I., Khim, B.K., Bak, Y.S., Lee, M.K., Lee, J., Domack, E.W., Christ, A.J., Yoon, H.I., 2018b. Holocene paleoceanography of Bigo Bay, west Antarctic Peninsula: connections between surface water productivity and nutrient utilization and its implication for surface-deep water mass exchange. Quat. Sci. Rev. 192, 59–70. https://doi.org/10.1016/j.quascirev.2018.05.028.
Lamb, A.L., Wilson, G.P., Leng, M.J., 2006. A review of coastal palaeoclimate and relative sea-level reconstructions using δ^{13}C and C/N ratios in organic material. Earth-Sci. Rev. 75, 29–57. https://doi.org/10.1016/j.earscirev.2005.10.003.
Lee, J.I., Bak, Y.S., Yoo, K.C., Lim, H.S., Yoon, H.I., Yoon, S.H., 2010. Climate changes in the south Orkney Plateau during the last 8600 years. Holocene 20 (30), 395–404.
Leventer, A., 1991. Sediment trap diatom assemblages from the northern Antarctic Peninsula region. Deep Sea Res. 38, 1127–1143.
Leventer, A., Domack, E., Barkoukis, A., McAndrews, B., Murray, J., 2002. Laminations from the Palmer Deep: A diatom-based interpretation. Paleoceanography 17, 8002. https://doi.org/10.1029/2001PA000624.
Leventer, A., Domack, E.W., Ishman, S.E., Brachfeld, S., McClennen, C.E., Manley, P.L., 1996. Productivity cycles of 200–300 years in the Antarctic Peninsula region: understanding linkages among the sun, atmosphere, oceans, sea ice, and biota. Geol. Soc. Am. Bull. 108, 1626–1644. https://doi.org/10.1130/0016-7606(1996)108<1626:PCOYIT>2.3.CO;2.
Lucchi, R.G., Rebesco, M., 2007. Glacial contourites on the Antarctic Peninsula margin: insight for palaeoenvironmental and palaeoclimatic conditions. In: Viana, A.R., Rebesco, M. (Eds.), Economic and Palaeoceanographic Significance of Contourite Deposits, vol. 276. Geological Society, London, Special Publications, pp. 111–127.
Lucchi, R.G., Rebesco, M., Camerlenghi, A., Busetti, M., Tomadin, L., Villa, G., Persico, D., Morigi, C., Bonci, M.C., Giorgetti, G., 2002. Mid-late Pleistocene glacimarine sedimentary processes of a high-latitude, deep-sea sediment drift (Antarctic Peninsula Pacific margin). Mar. Geol. 189, 343–370.
Maldonado, A., Barnolas, A., Bohoyo, F., Galindo-Zaldívar, Hernández-Molina, J., Lobo, F., Rodríguez-Fernández, Somoza, L., Vázquez, J.T., 2003. Contourite deposits in the central Scotia Sea: the importance of the antarctic circumpolar current and the Weddell Gyre flows. Palaeogeogr. Palaeoclimatol. Palaeoecol. 198, 187–221.
Manoj, M.C., Thamban, M., 2015. Shifting frontal regimes and its influence on bioproductivity variations during the Late Quaternary in the Indian sector of Southern Ocean. Deep-Sea Res. II 118, 261–274. https://doi.org/10.1016/j.dsr2.2015.03.011.
McCave, I.N., Andrews, J.T., 2019. Distinguishing current effects in sediments delivered to the ocean by ice, I. Principles, methods and examples. Quat. Sci. Rev. 212, 92–107. https://doi.org/10.1016/j.quascirev.2019.03.031.
McCave, I.N., Crowhurst, S.J., Kuhn, G., Hillenbrand, C.-D., Meredith, M.P., 2014. Minimal change in Antarctic Circumpolar Current flow speed between the last glacial and Holocene. Nat. Geosci. 7, 113–116. https://doi.org/10.1038/ngeo2037.
McCave, I.N., Manighetti, B., Robinson, S.G., 1995. Sortable silt and fine sediment size composition slicing–parameters for paleocurrent speed and paleoceanography. Paleoceanography 10, 593–610. https://doi.org/10.1029/94PA03039.
McCave, I.N., Thornalley, D.J.R., Hall, I.R., 2017. Relation of sortable silt grain size to deep-sea current speeds: calibration of the 'Mud Current Meter. Deep-Sea Res. I 127, 1–12. https://doi.org/10.1016/j.dsr.2017.07.003.
Merino, N., Le Sommer, J., Durand, G., Jourdain, N.C., Madec, G., Mathiot, P., Tournadre, J., 2016. Antarctic icebergs melt over the Southern Ocean: climatology and impact on sea ice. Ocean Model. 104, 99–110. https://doi.org/10.1016/j.ocemod.2016.05.001.
Mortlock, R.A., Froelich, P.N., 1989. A simple method for the rapid determination of opal in pelagic marine sediments. Deep-Sea Res. 36, 1415–1426.
Needoba, J.A., Waser, N.A., Harrison, P.J., Calvert, S.E., 2003. Nitrogen isotope fractionation in 12 species of marine phytoplankton during growth on nitrate. Mar. Ecol. Prog. Ser. 255, 81–91.
Nie, Y., Liu, X., Wen, T., Sun, L., Emslie, S.D., 2014. Environmental implication of nitrogen isotopic composition in ornithogenic sediments from the Ross Sea region, East Antarctica: Δ^{15}N as a new proxy for avian influence. Chem. Geol. 363, 91–100. https://doi.org/10.1016/j.chemgeo.2013.10.031.
Ó Cofaigh, C.O., Dowdeswell, J.A., Pudsey, C.J., 2001. Late quaternary iceberg rafting along the antarctic Peninsula continental rise and in the Weddell and Scotia seas. Quat. Res. 56, 308–321.
Orsi, A.H., Whitworth, T., Nowlini Jr., W.D., 1995. On the meridional extent and fronts of the Antarctic circumpolar current. Deep Sea Res. I 42 (5), 641–673.
Passchier, S., 2011. Linkages between East antarctic ice sheet extent and Southern Ocean temperatures based on a pliocene high-resolution record of ice-rafted debris off Prydz Bay, East Antarctica. Paleoceanography 26, PA4204. https://doi.org/10.1029/2010PA002061.
Patterson, M.O., McKay, R., Naish, T., Escutia, C., Jimenez-Espejo, F.J., Raymo, M.E., Meyers, S.R., Tauxe, L., Brinkhuis, H., IODP Expedition 318 Scientists, 2014. Orbital forcing of the east antarctic ice sheet during the pliocene and early pleistocene. Nat. Geosci. 7, 841–847. https://doi.org/10.1038/NGEO2273.
Pugh, R.S., MaCave, I.N., Hillenbrand, C.-D., Kuhn, G., 2009. Circum-Antarctic age modeling of Quaternary marine cores under the Antarctic Circumpolar Current: ice-core dust-magnetic correlation. Earth Planet Sci. Lett. 284, 113–123.
Reimer, P.J., Bard, E., Bayliss, A., Beck, J.W., Blackwell, P.G., Ramsey, C.B., Buck, C.E., Cheng, H., Edwards, R.L., Friedrich, M., Grootes, P.M., Guilderson, T.P., Haflidason, H., Hajdas, I., Hatté, C., Heaton, T.J., Hoffmann, D.L., Hogg, A.G., Hughen, K.A., Kaiser, K.F., Kromer, B., Manning, S.W., Niu, M., Reimer, R.W., Richards, D.A., Scott, E.M., Southon, J.R., Staff, R.A., Turney, C.S.M., van der Plicht, J., 2013. IntCal13 and Marine13 Radiocarbon age calibration curves 0-50,000 years cal BP. Radiocarbon 55, 1869–1887.
Roberts, J., McCave, I.N., McClymont, E.L., Kender, S., Hillenbrand, C.D., Matano, R., Hodell, D.A., Peck, V.L., 2017. Earth Planet Sci. Lett. 474, 397–408. https://doi.org/10.1016/j.epsl.2017.07.004.
Schubert, C.J., Calvert, S.E., 2001. Nitrogen and carbon isotopic composition of marine and terrestrial organic matter in Arctic Ocean sediments: implications for nutrient utilization and organic matter composition. Deep-Sea Res. I 48, 789–810.
Shin, J.Y., Kim, S., Zhao, X., Yoo, K.C., Yu, Y., Lee, J.I., Lee, M.K., Yoon, H.I., 2020. Particle-size dependent magnetic properties of Scotia Sea sediments since the Last Glacial Maximum: glacial ice-sheet discharge controlling magnetic proxeis. Palaeogeogr. Palaeoclimatol. Palaeoecol. 557, 109906. https://doi.org/10.1016/j.palaeo.2020.109906.
Socal, G., Noethig, E.M., Bianchi, F., Boldrin, A., Mathot, S., Rabitti, S., 1997.

Phytoplankton and particulate matter at the Weddell/Scotia Confluence (47°W) in summer 1989, as a final step of a temporal succession (EPOS project). Polar Biol. 18, 1–9.
Sprenk, D., Weber, M.E., Kuhn, G., Rosén, P., Frank, M., Molina-Kescher, M., Liebetrau, V., Röhling, H.G., 2013. Southern Ocean bioproductivity during the last glacial cycle—new detection method and decadal-scale insight from the Scotia Sea. Geol. Soc. London. Spec. Publ. 381, 245–261. https://doi.org/10.1144/SP381.17.
Studer, A.S., Sigman, D.M., Martínez-García, A., Benz, V., Winckler, G., Kuhn, G., Esper, O., Lamy, F., Jaccard, S.L., Wacker, L., Oleynik, S., Gersonde, R., Haug, G.H., 2015. Antarctic Zone nutrient conditions during the last two glacial cycles. Paleoceanography 30, 845–862. https://doi.org/10.1002/2014PA002745.
Stuiver, M., Reimer, P.J., 1993. Extended ^{14}C data base and revised CALIB 3.0 ^{14}C age calibration program. Radiocarbon 35, 215–230.
Tournadre, J., Bouhier, N., Girard-Ardhuin, F., Rmy, F., 2015. Large icebergs characteristics from altimeter waveforms analysis. J. Geophys. Res. 120, 1954–1974. https://doi.org/10.1002/2014JC010502.
Tréguer, P., Linder, L., van Bennekon, A.J., et al., 1991. Production of biogenic silica in the Weddell-Scotia Seas measured by using ^{32}Si. Limnol. Oceanogr. 36, 1217–1227.
Tréguer, P., Jacques, G., 1992. Dynamics of nutrients and phytoplankton, and fluxes of carbon, nitrogen and silicon in the Antarctic Ocean. Polar Biol. 12, 149–162.
Weber, M.E., Kuhn, G., Sprenk, D., Rolf, C., Ohlwein, C., Ricken, W., 2012. Dust transport from Patagonia to Antarctica—a new stratigraphic approach from the Scotia Sea and its implications for the last glacial cycle. Quat. Sci. Rev. 36, 177–188.
Weber, M.E., Clark, P.U., Kuhn, G., Timmermann, A., Sprenk, D., Gladstone, R., Zhang, X., Lohmann, G., Menviel, L., Chikamoto, M.O., Friedrich, T., Ohlwein, C., 2014. Millennial-scale variability in Antarctic ice-sheet discharge during the last deglaciation. Nature 510, 134–138.
Wu, L., Wang, R., Xiao, W., Krijgsman, W., Li, Q., Ge, S., Ma, T., 2018. Late Quaternary deep stratification-climate coupling in the Southern Ocean: implications for changes in abyssal carbon storage. G-cubed 19. https://doi.org/10.1002/2017GC007250.
Xiao, W., Frederichs, T., Gersonde, R., Kuhn, G., Esper, O., Zhang, X., 2016. Constraining the dating of late quaternary marine sediment records from the Scotia Sea (Southern Ocean). Quat. Geochronol. 31, 97–118. https://doi.org/10.1016/j.quageo.2015.11.003.
Yamazaki, T., Ikehara, M., 2012. Origin of magnetic mineral concentration variation in the Southern Ocean. Paleoceanography 27, PA2206. https://doi.org/10.1029/2011PA002271.
Yoon, H.I., Khim, B.K., Yoo, K.-C., Bak, Y.S., Lee, J.I., 2007. Late glacial to Holocene climatic and oceanographic record of sediment facies from the South Scotia Sea off the northern Antarctic Peninsula. Deep-Sea Res. II 54, 2367–2387.